Front. Eng. Manag. 2021, 8(1): 122–134
https://doi.org/10.1007/s42524-019-0072-x

RESEARCH ARTICLE

Xinzheng LU, Qingle CHENG, Zhen XU, Chen XIONG

Regional seismic-damage prediction of buildings under mainshock–aftershock sequence

Abstract Strong aftershocks generally occur following a significant earthquake. Aftershocks further damage buildings weakened by mainshocks. Thus, the accurate and efficient prediction of aftershock-induced damage to buildings on a regional scale is crucial for decision making for post-earthquake rescue and emergency response. A framework to predict regional seismic damage of buildings under a mainshock–aftershock (MS–AS) sequence is proposed in this study based on city-scale nonlinear time-history analysis (THA). Specifically, an MS–AS sequence-generation method is proposed to generate a potential MS–AS sequence that can account for the amplification, spectrum, duration, magnitude, and site condition of a target area. Moreover, city-scale nonlinear THA is adopted to predict building seismic damage subjected to MS–AS sequences. The accuracy and reliability of city-scale nonlinear THA for an MS–AS sequence are validated by as-recorded seismic responses of buildings and simulation results in published literature. The town of Longtoushan, which was damaged during the Ludian earthquake, is used as a case study to illustrate the detailed procedure and advantages of the proposed framework. The primary conclusions are as follows. (1) Regional seismic damage of buildings under an MS–AS sequence can be predicted reasonably and accurately by city-scale nonlinear THA. (2) An MS–AS sequence can be generated reasonably by the proposed MS–AS sequence-generation method. (3) Regional seismic damage of buildings under different MS–AS scenarios can be provided efficiently by the proposed framework, which in turn can provide a useful reference for earthquake emergency response and scientific decision making for earthquake disaster relief.

Keywords regional seismic damage prediction, city-scale nonlinear time-history analysis, mainshock–aftershock sequence, multiple degree-of-freedom (MDOF) model, 2014 Ludian earthquake

Received April 3, 2019; accepted September 11, 2019

Xinzheng LU (✉)
Key Laboratory of Civil Engineering Safety and Durability of China Education Ministry, Department of Civil Engineering, Tsinghua University, Beijing 100084, China
E-mail: luxz@tsinghua.edu.cn

Qingle CHENG
Beijing Engineering Research Center of Steel and Concrete Composite Structures, Tsinghua University, Beijing 100084, China

Zhen XU
Beijing Key Laboratory of Urban Underground Space Engineering, School of Civil and Resource Engineering, University of Science and Technology Beijing, Beijing 100083, China

Chen XIONG
Guangdong Provincial Key Laboratory of Durability for Marine Civil Engineering, Shenzhen University, Shenzhen 518060, China

The authors are grateful for the financial support received from the National Key R&D Program (Grant No. 2018YFC1504401) and the National Natural Science Foundation of China (Grant No. 51778341).

1 Introduction

1.1 Research background

Strong aftershocks generally occur following a significant earthquake, such as the 1976 Tangshan earthquake, the 2008 Wenchuan earthquake, the 2015 Gorkha earthquake, and the 2016 Central Italy earthquake (Zheng et al., 2010; Valensise et al., 2017; Varum et al., 2017; Wan et al., 2017). Structures damaged by a mainshock cannot be repaired in a short period of time, and aftershocks will cause further damage to buildings weakened by mainshocks, thereby resulting in severe consequences (e.g., the 2011 Christchurch earthquake (Potter et al., 2015), the 2015 Gorkha earthquake (Chen et al., 2017), and the 2016 Central Italy earthquake (Rinaldin and Amadio, 2018)). Therefore, the damage of buildings subjected to a mainshock–aftershock (MS–AS) sequence should be considered.

To date, the effect of aftershocks on different types of buildings (e.g., reinforced concrete (RC) frames (Jalayer

et al., 2011; Raghunandan et al., 2012; 2015; Hatzivassiliou and Hatzigeorgiou, 2015; Hosseinpour and Abdelnaby, 2017; Jalayer and Ebrahimian, 2017), wooden frames (Goda and Salami, 2014), steel frames (Ruiz-García and Negrete-Manriquez, 2011), RC shear wall-frame structures (Jamnani et al., 2018), etc.) has been investigated. In addition to damage prediction for individual buildings, aftershock-induced damage prediction of buildings on a regional scale is also important for post-earthquake decision making. However, no satisfactory solution is currently available for regional damage prediction of buildings under an MS–AS sequence.

1.2 Challenges for regional seismic-damage prediction of buildings under an MS–AS sequence

The following three key challenges must be addressed to realize regional seismic-damage prediction of buildings under an MS–AS sequence.

(1) A regional seismic-damage prediction method that can consider the effect of an aftershock

Existing regional seismic-damage prediction methods primarily include: (1) The damage probability matrix (DPM) method (Applied Technology Council, 1985; Yepes-Estrada et al., 2016), (2) the capacity spectrum method (CSM) (Federal Emergency Management Agency, 2012), and (3) the time-history analysis (THA)-based method (Lu and Guan 2017; Hori et al., 2018). The DPM method, which is based on the statistical damage of different types of structures in previous earthquakes, has been widely used for regional seismic-damage prediction (Onur et al., 2006). However, it cannot satisfy the demand of damage prediction subjected to MS–AS sequences owing to the limited historic data of building damage under such sequences. Meanwhile, the CSM was developed based on pushover analyses of single-degree-of-freedom (SDOF) building models. Although damage accumulation can be considered in pushover analysis (Polese et al., 2013), the influence of higher-order vibration modes and several characteristics of ground motions (e.g., different durations or velocity pulses) cannot be considered easily by the CSM (Lu et al., 2014).

Based on the multiple-degree-of-freedom (MDOF) model and nonlinear THA, the regional seismic-damage prediction method proposed by Lu and Guan (2017) (hereinafter referred to as "city-scale nonlinear THA") can well consider the characteristics of different ground motions and buildings. Specifically, this method can adopt an MS–AS sequence as the ground motion input of building models for THA, thereby enabling the prediction of regional seismic damage of buildings under an MS–AS sequence. However, no existing work can be found in the literature on the application of city-scale nonlinear THA for regional damage prediction of buildings under an MS–AS sequence.

(2) Validation of the accuracy of the adopted method subjected to an MS–AS sequence

Ensuring the accuracy and reliability of prediction methods for building seismic damage is critical. The city-scale nonlinear THA proposed by Lu and Guan (2017) has been validated through the comparison of simulation results with actual seismic responses, experimental results, and a large number of numerical results (Xu et al., 2014; Xiong et al., 2016; 2017). Theoretically, this method can be applied to building MS–AS analysis; however, further validation of its accuracy is necessary.

The Center for Engineering Strong Motion Data (CESMD) (Haddadi et al., 2012) provides a considerable number of valuable actual building seismic responses under multiple earthquakes as well as building inventories required to determine MDOF model parameters for city-scale nonlinear THA. Meanwhile, numerous existing studies (Ruiz-García and Negrete-Manriquez, 2011; Hatzivassiliou and Hatzigeorgiou, 2015; Ruiz-García et al., 2018) have provided numerical responses of individual buildings under an MS–AS sequence, which can be used to validate city-scale nonlinear THA.

(3) MS–AS sequence-generation method

An MS–AS sequence is required as the input of MDOF models for the nonlinear THA of buildings. Thus, a rational MS–AS sequence-generation method is the foundation of regional seismic-damage prediction of buildings. At present, the MS–AS sequence-generation method primarily includes the following:

a) As-recorded MS–AS sequences (Ruiz-García and Negrete-Manriquez, 2011; Hatzivassiliou and Hatzigeorgiou, 2015; Zhai et al., 2014; 2016). However, this method is not suitable for seismic-damage prediction of buildings under different MS–AS scenarios owing to the large differences between the MS–AS mechanisms of different earthquakes and limited as-recorded MS–AS sequences.

b) Artificially generated MS–AS sequence. The simplest method to artificially generate an MS–AS sequence is to repeat a mainshock ground motion using scaled peak ground acceleration (PGA) as the aftershock ground motion (Amadio et al., 2003; Fragiacomo et al., 2004; Hatzigeorgiou and Beskos, 2009). The PGA of a generated aftershock ground motion is determined by historic MS–AS sequence data regression. However, the entire time history of an aftershock can hardly be simulated with scaled mainshock ground motions owing to the considerable magnitude difference between a mainshock and an aftershock. Thus, a rational solution would be to generate aftershock ground motions considering more key parameters (e.g., earthquake magnitude, response spectrum, rupture distance, and site condition, etc.) in addition to PGA. Previous studies have proposed various models that consider the acceleration spectrum (Li and Ellingwood, 2007), magnitude, PGA (Goda and Taylor, 2012), epicenter distance, site conditions (Goda, 2012), and site condition and aftershock characteristics (Hu et al., 2018). However, further improvement is still required to

encompass more key parameters in the model.

1.3 Overview of the study

In this work, a framework predicting the regional seismic-damage of buildings under an MS–AS sequence is proposed to address the three abovementioned challenges. Specifically, city-scale nonlinear THA is adopted to implement building seismic damage subjected to MS–AS sequences. Simulation results are validated through the comparison of as-recorded seismic responses of buildings and simulated building responses in published literature. An MS–AS sequence-generation method that covers more key parameters (e.g., amplification, spectrum, duration, magnitude, and site condition) is proposed. Thus, various MS–AS sequences can be generated by the proposed method. Subsequently, the regional-scale scenarios of buildings subjected to different MS–AS sequences can be predicted. Finally, the town of Longtoushan, which was damaged during the Ludian earthquake, is used as a case study to predict building damage subjected to different MS–AS sequences to illustrate the detailed procedure and advantages of the proposed framework.

2 Regional seismic-damage prediction of buildings under an MS–AS sequence

2.1 Proposed framework

The proposed framework for predicting the regional seismic-damage of buildings under an MS–AS sequence is illustrated in Fig. 1. The process consists of five steps.

(1) The ground motion record of a mainshock near the epicenter can be obtained quickly after an earthquake by densely distributed strong-motion stations. Moreover, information such as magnitude, station location, and fault parameters can be collected simultaneously.

(2) Allowing for the uncertainty of the times, locations, and magnitudes of aftershocks, a series of aftershock scenarios that assume different magnitudes, locations, and fault parameters are generated.

(3) The amplitude, response spectrum, and duration of aftershocks are estimated based on the generated aftershock scenarios by the proposed MS–AS sequence-generation method.

(4) Ground motions are selected from the NGA-West2 ground motion database (Ancheta et al., 2014) as the ground motions of an aftershock. The selected ground motions have similar magnitude, amplification, spectrum, duration, and site conditions as a target aftershock.

(5) The ground motions of MS–AS sequences are generated using recorded mainshock ground motions and predicted aftershock ground motions. City-scale nonlinear THA is implemented using the ground motions of MS–AS sequences and the building inventory of a target region. Thus, regional seismic damage of buildings subjected to MS–AS sequences can be predicted.

2.2 Regional seismic-damage prediction method

Based on the nonlinear MDOF model and THA analysis, the city-scale nonlinear THA proposed by Lu and Guan (2017) is adopted in this work to predict regional seismic

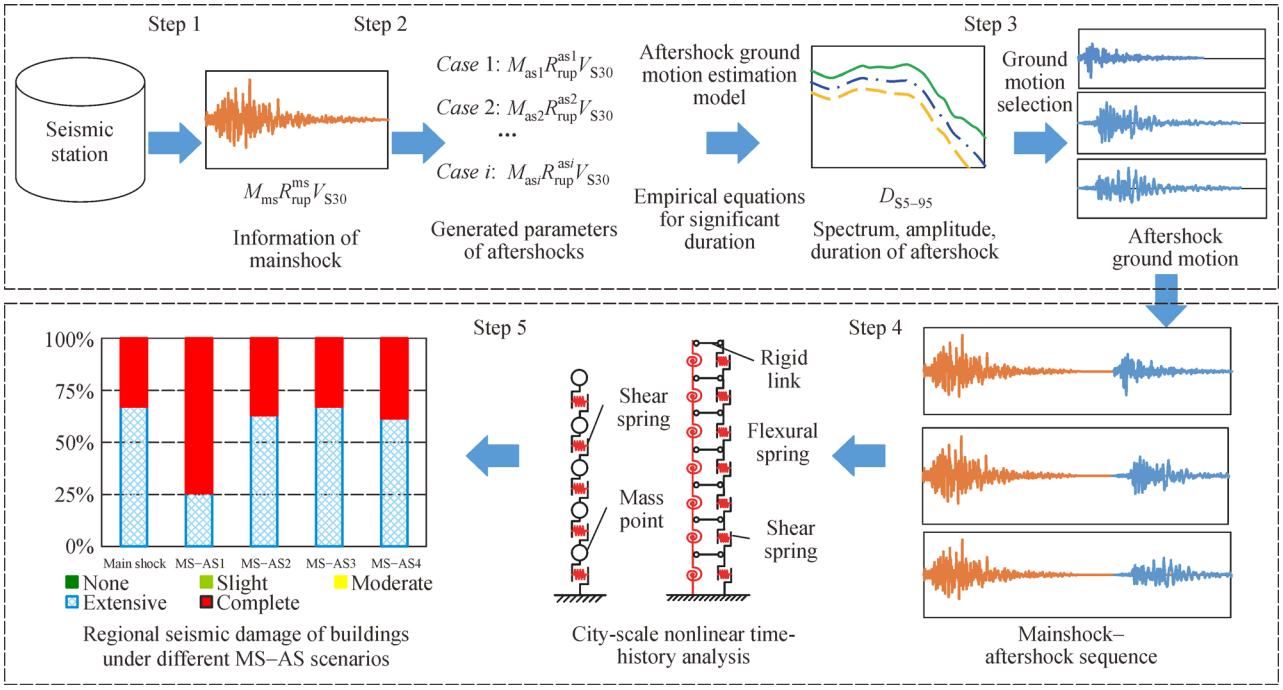

Fig. 1 Framework for predicting regional seismic damage of buildings under an MS–AS sequence.

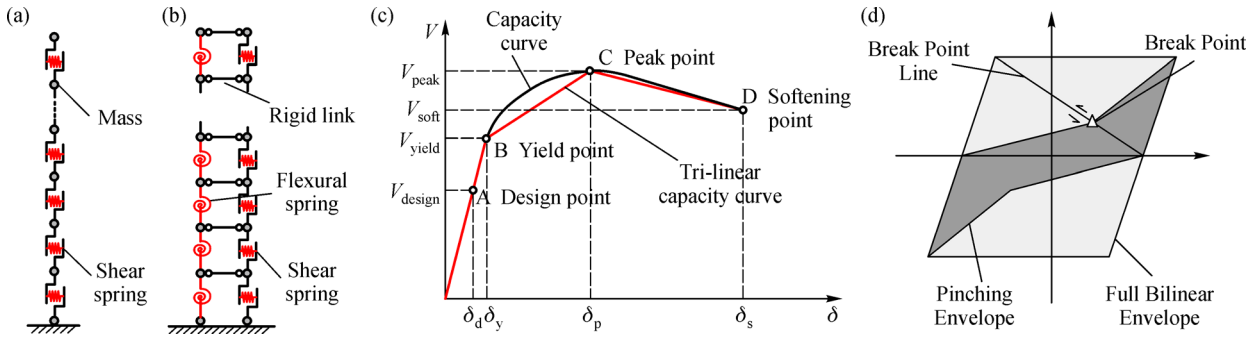

Fig. 2 (a) Nonlinear MDOF shear model; (b) MDOF flexural–shear model; (c) tri-linear backbone curve; and (d) single-parameter hysteretic model used in city-scale nonlinear THA (Lu and Guan, 2017).

damage of buildings. Generally, buildings in a target region can be primarily divided into ordinary multistory buildings and ordinary tall buildings (Xiong et al., 2016; 2017). Multistory buildings generally exhibit shear deformation modes under earthquakes, whereas tall buildings will deform in flexural–shear modes. Therefore, the MDOF shear model (Fig. 2a) and the MDOF flexural–shear model (Fig. 2b) are used for multistory buildings and tall buildings, respectively.

In terms of the MDOF model, the mass of the buildings is concentrated on their corresponding stories, and the nonlinear behavior of the structure is represented by nonlinear inter-story force–displacement relationships (Fig. 2c). The single-parameter pinching model (Fig. 2d) proposed by Steelman and Hajjar (2009) is adopted to represent pinching behavior subjected to cyclic loads. Lu and Guan (2017) proposed a model parameter-determination method for multistory and tall buildings on the basis of the design process specified in design codes and abundant experimental and numerical data. Based on building inventory data (i.e., floor area, number of stories, height, structural type, year built, and function), the MDOF models of buildings can be established automatically through this method. The time histories of the seismic response (i.e., acceleration, velocity, and displacement) of each story in every building can be obtained by conducting nonlinear THA of MDOF models. The five damage states (i.e., none, slight, moderate, extensive, and complete) of each building are determined based on inter-story displacement and force. The reliability of this method has been already validated through the comparison of simulation results of earthquake site investigations, experimental results, and a large number of numerical results (Lu and Guan, 2017).

2.3 Validation of city-scale nonlinear THA subjected to an MS–AS sequence

The accuracy and reliability of city-scale nonlinear THA subjected to an MS–AS sequence are validated in this section by the as-recorded seismic responses of buildings and simulation results in published literature.

2.3.1 Comparison with as-recorded seismic responses of buildings

The as-recorded seismic responses of buildings under an MS–AS sequence in the CESMD database (Haddadi et al., 2012) are collected to validate city-scale nonlinear THA. The MDOF model parameters of each building are determined by the parameter-determination method based on building inventories (Lu and Guan, 2017). The responses of buildings under an MS–AS sequence are calculated by inputting as-recorded ground motions into the MDOF models. The details of the buildings and the MS–AS sequences are listed in Table 1. Structural types are classified based on HAZUS (Federal Emergency Management Agency, 2012) building classes. The results are compared with actual responses obtained from the CESMD database, as shown in Fig. 3. A typical comparison of roof displacement histories for building #3 in Table 1 is shown in Fig. 4. The simulation results agree well with actual observations. It should be noted that some seismic events have low magnitudes owing to the limited as-recorded seismic response of buildings under an MS–AS sequence.

2.3.2 Comparison with simulation results in published literature

To further validate the reliability of the MDOF models proposed by Lu and Guan (2017) in predicting seismic responses of buildings under an MS–AS sequence, the results of the MDOF models are compared with the simulation results of buildings provided in the published literature. Building information and MS–AS sequences are listed in Table 2. Further details can be found in the corresponding literature. Eight sets of comparison results for buildings with steel frame are given, as shown in Fig. 5, in which the *x*-axis and *y*-axis are inter-story drift ratios

Table 1 Information of buildings and MS–AS

ID	Building name	Mainshock (M_w)	Aftershock (M_w)	Number of stories	Structural type	Year built	PGA of MS (m/s^2)	PGA of AS (m/s^2)
1	Bishop two-story office building	M4.8 Big Pine earthquake of 16 Feb 2016	M4.3 Big Pine earthquake of 16 Feb 2016	2	S1L	1976	0.06	0.05
2	Oakland 11-story residential building	M4.0 Berkeley earthquake of 20 Oct 2011	M3.8 Berkeley earthquake of 20 Oct 2011	11	C2H	1972	0.53	0.63
3	Walnut Creek 10-story commercial building	M5.9 Livermore earthquake of 24 Jan 1980	M5.8 Livermore earthquake of 26 Jan 1980	10	C2H	1970	0.29	0.54
4	Walnut Creek 10-story commercial building	M4.0 Berkeley earthquake of 20 Oct 2011	M3.8 Berkeley earthquake of 20 Oct 2011	10	C2H	1970	0.07	0.07
5	Fortuna one-story supermarket building	M7.1 Petrolia earthquake of 25 Apr 1992	M6.5 Petrolia aftershock 1 of 26 Apr 1992	1	RM1L	1979	1.36	1.57
6	Oakland 24-story residential building	M4.0 Berkeley earthquake of 20 Oct 2011	M3.8 Berkeley earthquake of 20 Oct 2011	24	C2H	1964	0.22	0.17
7	Berkeley two-story hospital	M4.0 Berkeley earthquake of 20 Oct 2011	M3.8 Berkeley earthquake of 20 Oct 2011	2	S2L	1984	0.62	0.38
8	Piedmont three-story school office building	M4.0 Berkeley earthquake of 20 Oct 2011	M3.8 Berkeley earthquake of 20 Oct 2011	3	C2L	1973	0.35	0.29
9	Oakland three-story commercial building	M4.0 Berkeley earthquake of 20 Oct 2011	M3.8 Berkeley earthquake of 20 Oct 2011	3	S5L	1972	0.18	0.27
10	San Francisco six-story gov office building	M4.0 Berkeley earthquake of 20 Oct 2011	M3.8 Berkeley earthquake of 20 Oct 2011	6	S5M	1987	0.25	0.29

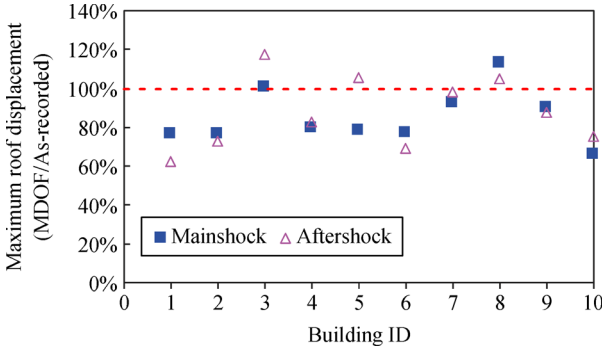

Fig. 3 Comparison between as-recorded seismic responses and results calculated by MDOF models.

(IDRs) calculated by the MDOF model and provided in published literature, respectively. Typical comparisons for buildings with IDs 1, 2, and 7 are shown in Fig. 6. The maximum floor displacement of a three-story RC frame with IDs 9 and 10 in Table 2 under an MS–AS sequence and a mainshock are further compared, respectively, as shown in Fig. 7. The average ratio between the predicted IDRs and the values provided in the literature is 1.08, with a coefficient of variations of 0.22. The simulation results of the MDOF model agree well with the results provided in published literature.

The comparisons in Sections 2.3.1 and 2.3.2 above demonstrate that city-scale nonlinear THA based on the MDOF models can accurately predict building responses subjected to an MS–AS sequence.

2.4 MS–AS sequence generation method

To determine the suitable ground motions for the MS–AS

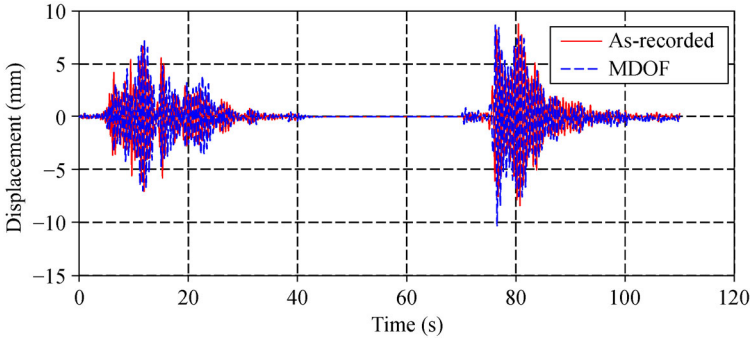

Fig. 4 Comparison of roof displacement histories for building #3 shown in Table 1.

Table 2 Building information and MS–AS sequences selected from the literature

ID	Number of stories	Structural type	MS–AS information	References
1	20	Steel frame	2010/2011 Canterbury earthquakes	Ruiz-García et al. (2018)
2	3	Steel frame	1980 Mammoth Lakes earthquakes	
3	9	Steel frame	1980 Mammoth Lakes earthquakes	
4	3	Steel frame	2011 Tohoku earthquakes	
5	9	Steel frame	2011 Tohoku earthquakes	
6	4	Steel frame	1980 Mammoth Lakes earthquakes	Ruiz-García and Negrete-Manriquez (2011)
7	8	Steel frame	1980 Mammoth Lakes earthquakes	
8	12	Steel frame	1980 Mammoth Lakes earthquakes	
9	3	RC frame	Imperial Valley earthquakes (MS–AS)	Hatzivassiliou and Hatzigeorgiou (2015)
10	3	RC frame	Imperial Valley earthquake (mainshock)	

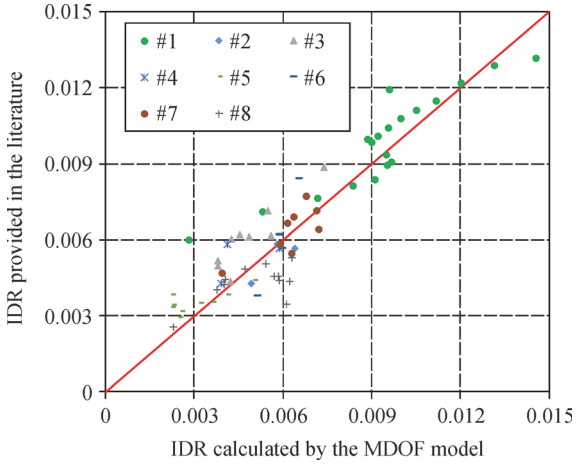

Fig. 5 Comparison of IDRs provided in the literature and calculated by the MDOF model for buildings with steel frame shown in Table 2.

sequence analysis, a scenario-based MS–AS sequence-generation method is proposed herein.

2.4.1 Determination of the amplitude and response spectrum of an aftershock

Kim and Shin (2017) proposed an empirical model to estimate the intensity measures of an aftershock using MS–AS paired records at the same stations from the NGA-West2 database. This model is adopted to determine the amplitude and spectral acceleration of an aftershock, which is shown in Eqs. (1)–(4).

$$\ln\left(\frac{Y^{\mathrm{AS}}}{Y^{\mathrm{MS}}}\right)=f_{\mathrm{mag}}+f_{\mathrm{dist}}+f_{\mathrm{site}}, \tag{1}$$

$$f_{\mathrm{mag}}=\begin{cases} c_0+c_1\left(M_{\mathrm{w}}^{\mathrm{AS}}/M_{\mathrm{w}}^{\mathrm{MS}}\right) & M_{\mathrm{w}}^{\mathrm{AS}}/M_{\mathrm{w}}^{\mathrm{MS}}\geqslant 0.75 \\ c_2+c_3\left(M_{\mathrm{w}}^{\mathrm{AS}}/M_{\mathrm{w}}^{\mathrm{MS}}\right) & M_{\mathrm{w}}^{\mathrm{AS}}/M_{\mathrm{w}}^{\mathrm{MS}}<0.75 \end{cases}, \tag{2}$$

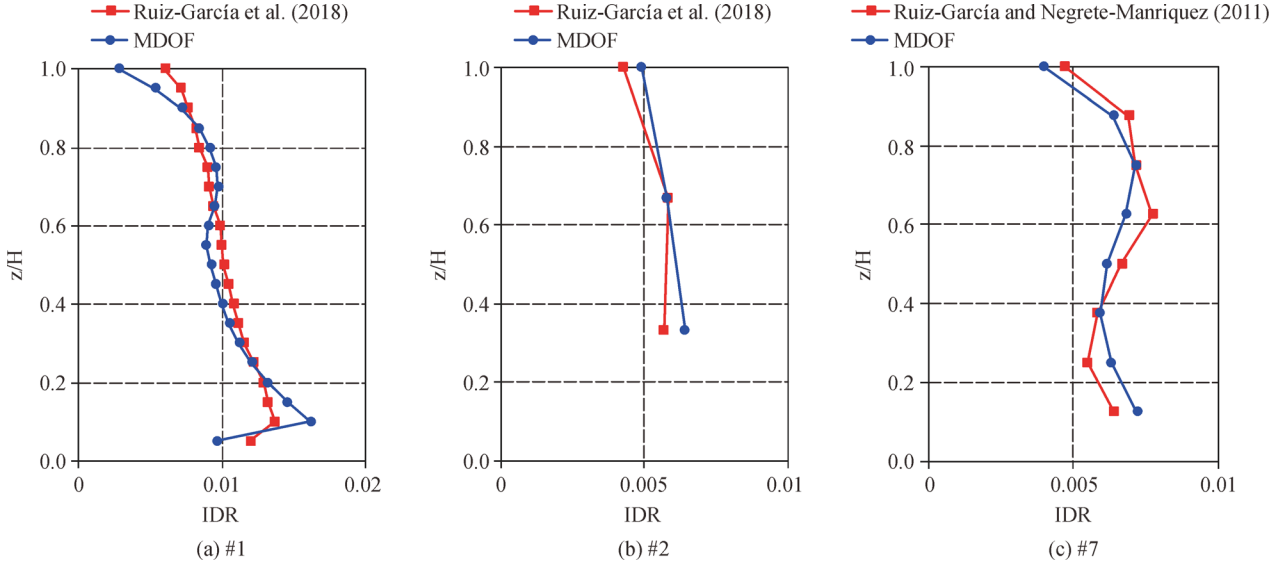

Fig. 6 Typical comparisons of IDRs provided in the literature and calculated by the MDOF model for buildings #1, #2, and #7 shown in Table 2.

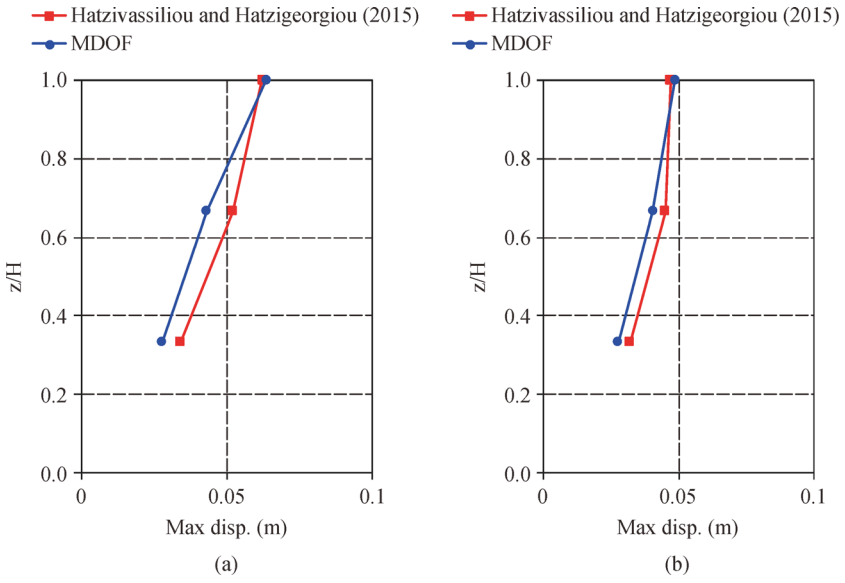

Fig. 7 Comparison of responses for the RC frame (buildings #9 and #10 shown in Table 2) under (a) an MS–AS sequence and (b) a mainshock, respectively.

$$f_{\text{dist}} = \left(c_4 + c_5 \ln\left(\frac{R_{\text{rup}}^{\text{AS}}}{R_{\text{rup}}^{\text{MS}}}\right)\right)\left(1 - \frac{M_{\text{w}}^{\text{AS}}}{M_{\text{w}}^{\text{MS}}}\right), \quad (3)$$

$$f_{\text{site}} = \left(c_6 \ln(V_{\text{S30}})\right)\left(1 - \frac{M_{\text{w}}^{\text{AS}}}{M_{\text{w}}^{\text{MS}}}\right), \quad (4)$$

where Y represents a ground motion intensity measure (e.g., PGA, peak ground velocity (PGV), and 5% damped pseudo spectral accelerations (PSAs)). It is noteworthy that these ground motion intensity measures are the orientation-independent measure of ground motion referred to as RotD50, which is the 50th percentile of the two measures over all non-redundant rotation angles (Kim and Shin, 2017). The superscripts AS and MS denote aftershock and mainshock, respectively; f_{mag}, f_{dist}, and f_{site} represent the functions for magnitude ratio, distance ratio, and site condition, as expressed in Eqs. (2)–(4); M_{w}, R_{rup}, and V_{S30} are moment magnitude, the closest distance from the fault rupture, and time-averaged shear-wave velocities for the top 30 m soil deposits, respectively; and c_0 to c_6 are regression coefficients. Among them, V_{S30} can be determined before an earthquake, and magnitude and distance parameters can be obtained based on the magnitudes, locations, and fault information of the mainshock and aftershock. The details of the model can be found in Kim and Shin (2017). Two sets of PSAs computed by this model are compared with as-recorded MS–AS sequences (Goda and Taylor, 2012) to validate accuracy, as shown in Fig. 8. The simulation results agree well with the as-recorded PSAs. It should be noted that the aftershock spectrum-prediction method used in this work can be replaced by other aftershock spectrum-prediction methods.

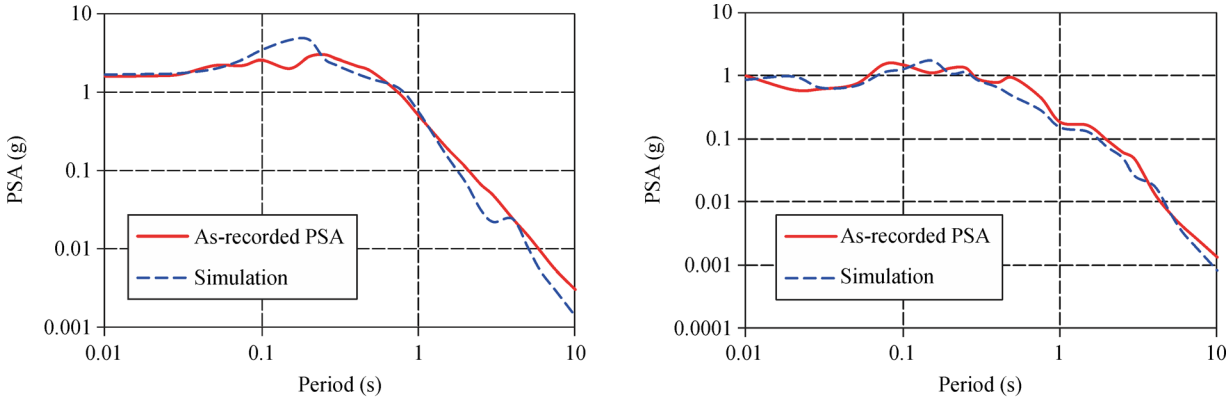

Fig. 8 Comparison between as-recorded PSAs and simulation results.

2.4.2 Determination of the significant duration of an aftershock

Duration is a key parameter used to describe the features of ground motion. Numerous definitions of ground motion duration exist in the literature (Bommer and Martínez-Pereira, 1999), and the widely used significant duration (Du and Wang, 2017) is adopted in this study.

The empirical equations used to predict the significant duration proposed by Bommer et al. (2009) based on magnitude, the depth to the top of the rupture, and shear-wave velocity are used to determine the significant duration of an aftershock. Based on the NGA-West ground motion database (Chiou et al., 2008), the regression model for predicting the significant duration is given in Eq. (5).

$$\ln D_{\mathrm{S}} = c_0 + m_1 M_{\mathrm{w}} + (r_1 + r_2 M_{\mathrm{w}}) \ln \sqrt{R_{\mathrm{rup}}^2 + h_1^2} + v_1 \ln(V_{\mathrm{S30}}) + z_1 Z_{\mathrm{tor}}, \tag{5}$$

where D_{S} is the significant duration, and the typically used $D_{\mathrm{S5–95}}$ (the time interval between 5%–95% of the Arias intensity) is adopted in this work; Z_{tor} is the depth to the top of the rupture; and c_0, m_1, r_1, r_2, h_1, v_1, and z_1 are the regression coefficients. The details of the regression model can be found in Bommer et al. (2009).

2.4.3 Selection of ground motion to generate an MS–AS sequence

Ground motions with parameters close to a target aftershock can be selected as aftershock ground motions after the amplitude, response spectrum, and duration of the aftershock are determined. The selection of ground motion can be implemented in the NGA-West2 ground motion database (Ancheta et al., 2014) by using its online ground motion selection tool (Pacific Earthquake Engineering Research Center (PEER), 2019). An MS–AS sequence can be generated using the proposed method, which provides the input ground motion for the regional seismic-damage prediction of buildings under an MS–AS sequence.

Table 3 Mainshock and aftershock information of the 2011 Berkeley earthquake

	Magnitude M_{w}	Location	Focal depth (km)
Mainshock	4.0	37.86 N, 122.25 W	8.0
Aftershock	3.8	37.87 N, 122.25 W	9.6

Multiple sets of ground motion records can be selected as the aftershock for each analysis through which uncertainty caused by the input ground motion can be represented. The computational efficiency of the MDOF models adopted in this work can easily handle the computational cost owing to multiple ground motion inputs.

2.4.4 Actual MS–AS scenario to validate the MS–AS sequence-generation method

An M_{w} 4.0 earthquake struck Berkeley, California on October 20, 2011. Approximately five hours later, an M_{w} 3.8 earthquake struck Berkeley again, which was considered as an aftershock of the first earthquake (Wooddell and Abrahamson, 2014). This actual MS–AS scenario (i.e., the 2011 Berkeley M4.0–M3.8 earthquake (CESMD, 2019a; 2019b), as listed in Table 1) is selected to validate the proposed MS–AS sequence-generation method.

(1) First, the basic information of the mainshock and aftershock can be obtained easily, as listed in Table 3. The ground motions and structural seismic responses of both earthquakes are recorded on an 11-story building (i.e., the Oakland Residential Building (ORB) station). The ground motion records are shown in Fig. 9.

(2) Given the basic information of the aftershock, the estimated significant duration $D_{\mathrm{S5–95}}$ of the aftershock at this station is 3.08 s using Eq. (5). The $D_{\mathrm{S5–95}}$ of the actual aftershock ground motion record is 2.66 s, and the error of $D_{\mathrm{S5–95}}$ given by Eq. (5) is 15.8%.

(3) The response spectrum of the aftershock at the ORB station can be estimated by inputting the basic information of an MS–AS sequence into Eqs. (1)–(4), which is close to

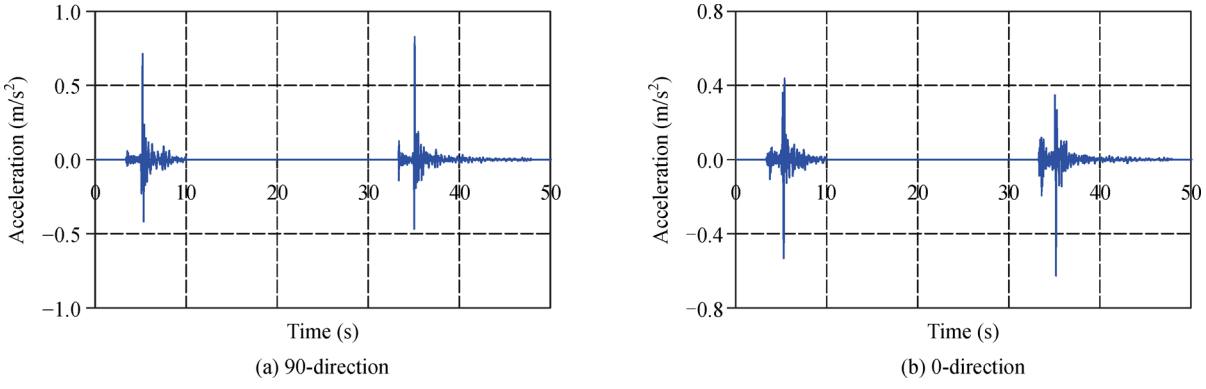

(a) 90-direction (b) 0-direction

Fig. 9 Ground motions recorded at the ORB station.

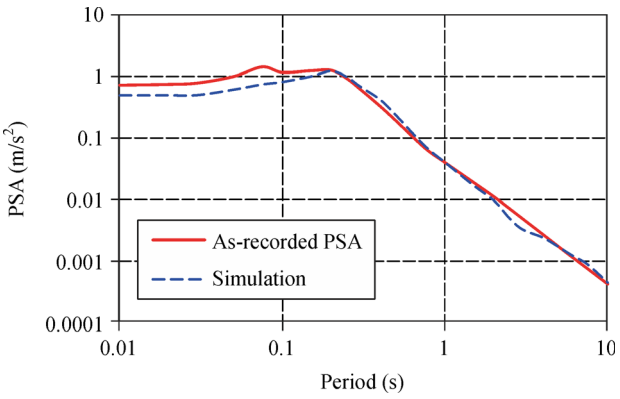

Fig. 10 Comparison between the predicted and actual response spectrum of ground motion recorded at the ORB station.

the response spectrum of the actual ground motion record, as apparent in Fig. 10.

(4) The ground motions of the aftershock can be selected from the NGA-West2 database after the key parameters of the aftershock are determined. A total of 15 ground motion sets is selected, as shown in Fig. 11.

(5) The ground motion of the mainshock and aftershock are linked together to generate MS–AS sequences, and a sufficiently long time interval with an acceleration equal to 0 (greater than 20 s) is added between the mainshock and aftershock to ensure that the structure is static before being subjected to the aftershock. Structural seismic responses can be obtained by inputting generated and actual MS–AS sequences into the MDOF model of the building. The error between the average maximum roof displacement, which is calculated using 15 MS–AS sequence sets, and the maximum roof displacement, which is calculated using an actual MS–AS sequence, is 11.54%. Thus, the results prove the reliability of the proposed MS–AS sequence-generation method.

3 Case study: Seismic-damage prediction of buildings in Longtoushan damaged in the Ludian earthquake

Buildings in Longtoushan damaged in the 2014 Ludian earthquake are selected as a case study to illustrate the detailed procedures and advantages of the proposed regional seismic-damage prediction of buildings under an MS–AS sequence.

The M_w 6.1 Ludian earthquake struck Longtoushan, Ludian County, China on August 3, 2014. The epicenter of this earthquake was near Longtoushan. The necessary inventories and damage information of 56 buildings, including RC frame, reinforced masonry (RM), and unreinforced masonry (URM) structures, are collected from the post-earthquake field investigation of Longtoushan (Xiong et al., 2017).

Buildings are simulated using the MDOF models. The MDOF model parameters of each building are determined by the corresponding parameter-determination method according to the number of stories, building height, structural type, year built, and planar area (Xiong et al., 2017). The damage of the buildings subjected to recorded mainshock ground motions is predicted by city-scale nonlinear THA. The predicted damage agrees well with actual damage states obtained from the field investigation (Xiong et al., 2017), which indicates the accuracy and reliability of city-scale nonlinear THA in predicting regional seismic damage. Based on this finding, the detailed procedure of the proposed framework to predict

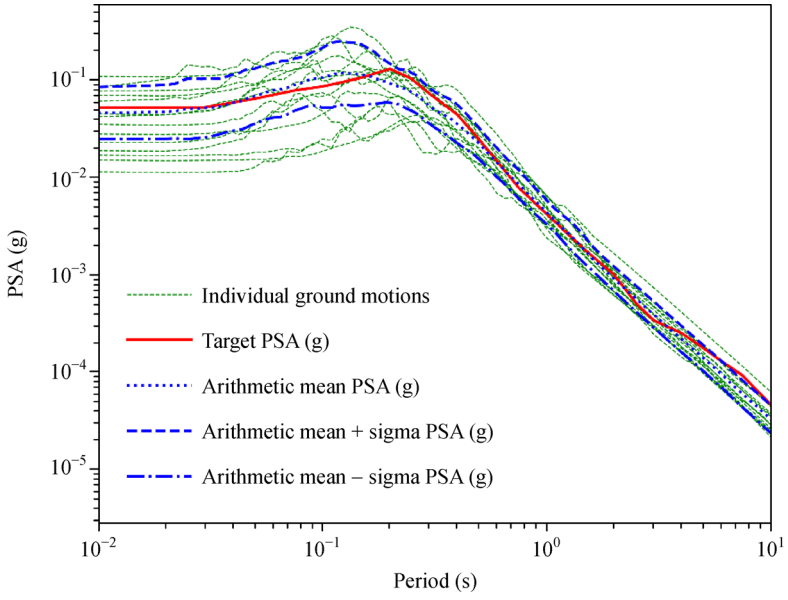

Fig. 11 Target response spectrum and the response spectrum of the selected ground motions.

Table 4 Mainshock and aftershock information

	Magnitude (M_w)	Rupture distance (km)	Focal depth (km)	Significant duration $D_{S5–95}$ (s)
Mainshock	6.1	14.9	12.0	-
Aftershock 1	6.1	14.9	12.0	5.55
Aftershock 2	5.5	14.9	12.0	4.57
Aftershock 3	5.0	14.9	12.0	3.73
Aftershock 4	5.5	13.0	12.0	4.28

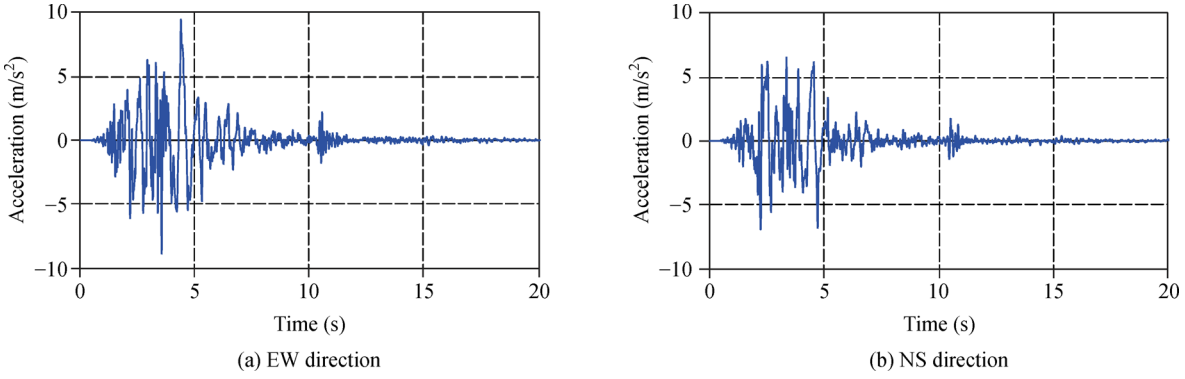

Fig. 12 Ground motions recorded at Longtoushan station.

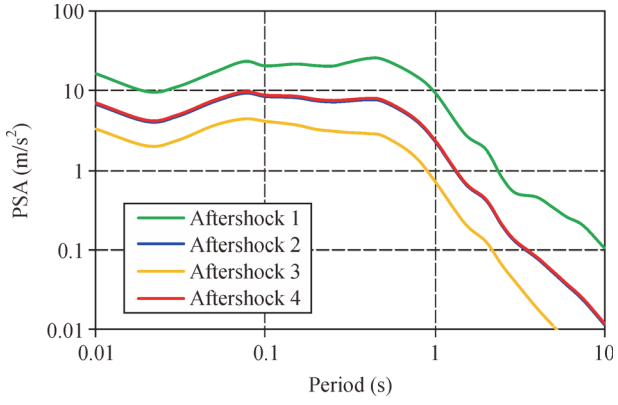

Fig. 13 Response spectrums of different aftershocks.

the regional seismic damage of buildings under an MS–AS sequence is introduced as follows.

(1) First, four aftershock scenarios are generated as a demonstration. The basic information of the mainshock and generated aftershocks are listed in Table 4. The mainshock ground motions recorded in Longtoushan are given in Fig. 12.

(2) Given the basic information of the aftershock, the significant duration $D_{S5–95}$ for each aftershock is estimated using Eq. (5), as listed in Table 4.

(3) The response spectrum for each generated aftershock can be estimated by inputting the basic information of an MS–AS sequence into Eqs. (1)–(4), as shown in Fig. 13.

(4) The ground motions of the aftershocks can be selected from the NGA-West2 database after the key parameters of the aftershocks are determined. A total of 20 ground motion sets is selected for each aftershock scenario to reduce the uncertainty of the building seismic response.

(5) The ground motions of the mainshock and aftershocks are linked together to generate MS–AS sequences, and a sufficiently long time interval with an acceleration equal to 0 (greater than 20 s) is added to ensure that the structure is static before being subjected to the aftershock. The regional seismic damage of buildings subjected to MS–AS sequences can be predicted by inputting generated MS–AS sequences into each building. The results of the mainshock and different MS–AS scenarios are compared, as shown in Fig. 14. The average damage ratio of 20 ground motion sets for each MS–AS scenario is given in Fig. 14(a). It is noteworthy that only two damage states, namely, "extensive damage" and "complete damage" occur in this case study. The standard deviations of the "complete damage" ratio under different scenarios can also be given, as shown in Fig. 14(b). Figure 14 shows that the aftershock's effect on the building is reduced simultaneously when its magnitude decreases. A comparative study between the results of generated and artificial seismic sequences has been conducted. The ground motion of a mainshock is repeated to generate an artificial seismic sequence, as indicated by "MS–MS" in Fig. 14(a). The artificial seismic sequence will cause more damage compared with the MS–AS 1 scenario, which is consistent with the investigations of Ruiz-García and Negrete-Manriquez (2011).

Figure 15 demonstrates that the seismic damage results of buildings with different structural types can be obtained.

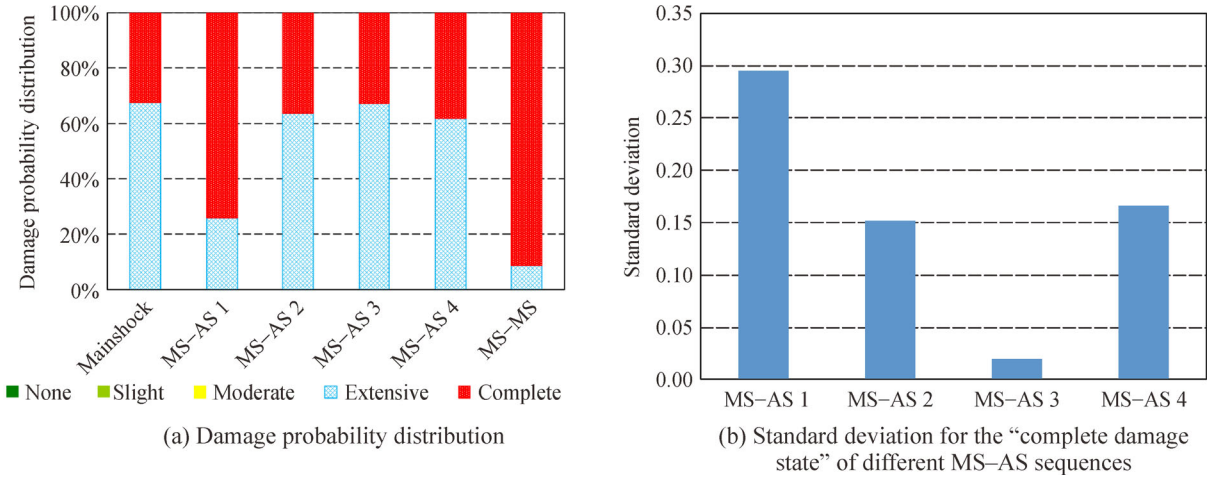

Fig. 14 Seismic damage results of buildings for different earthquake scenarios.

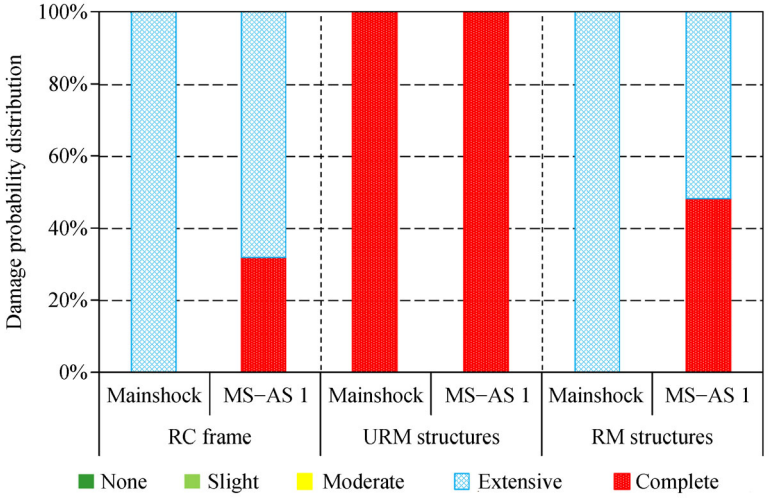

Fig. 15 Seismic damage results of buildings with different structural types.

Table 5 Maximum IDR and damage states of typical buildings

ID	Structural type	Number of stories	Mainshock	MS–AS 1	MS–AS 2	MS–AS 3	MS–AS 4
1	RM2L	3	0.0206	0.0474	0.0231	0.0206	0.0232
			Extensive	Complete	Extensive	Extensive	Extensive
2	RM2L	2	0.0203	0.0452	0.0226	0.0203	0.0227
			Extensive	Complete	Extensive	Extensive	Extensive

RM structures in Longtoushan will experience more damage than RC frames under MS–AS 1 scenario. The structural responses of individual buildings under different MS–AS scenarios can also be obtained using the proposed framework. For example, the maximum IDR and the damage states of two typical buildings in Longtoushan under different MS–AS scenarios are listed in Table 5 (buildings #1 and #2), which clearly demonstrate the consequences of different aftershocks to both buildings.

The predicted regional seismic damage of buildings under different MS–AS scenarios can provide a useful reference for earthquake emergency response and decision making for earthquake disaster relief. For example, according to Table 4 and Fig. 14, the following conclusions can be drawn preliminarily: Buildings in an earthquake-stricken area will not incur further damage in the event of an aftershock with a magnitude less than 5.0, and the existing disaster relief plan can be performed continuously. By contrast, an aftershock with a magnitude greater than 5.5 will cause further seismic damage to buildings; thus,

rescue forces and supplies should be increased correspondingly based on additional damages caused by the aftershock. It should be noted that these preliminary conclusions are based on the four assumed scenarios in the case study. Additional sophisticated conclusions require further comprehensive analysis with a large scenario database.

The calculation of an MS–AS scenario (with an Intel Xeon E5 2630 @ 2.40 GHz and 64 GB RAM) requires only 70 s, thereby indicating high computational efficiency. Consequently, regional seismic-damage prediction of buildings under the MS–AS sequence proposed in this work can satisfy the post-earthquake emergency response requirement. A variety of MS–AS scenarios can be quickly constructed after an earthquake, and the corresponding seismic damage of buildings can be obtained. An aftershock scenario with magnitude, location, and fault parameters closest to an actual aftershock can be chosen from the scenario database once an aftershock occurs. This scenario could then provide a useful reference for earthquake emergency response and decision making for earthquake disaster relief.

4 Conclusions

A framework for regional seismic-damage prediction of buildings under an MS–AS sequence was proposed in this study. City-scale nonlinear THA was adopted to simulate regional seismic damage of buildings under an MS–AS sequence. The accuracy and reliability of city-scale nonlinear THA were validated with as-recorded seismic responses of buildings and simulation results in published literature. Moreover, an MS–AS sequence-generation method was proposed to provide input ground motion by determining the key parameters (i.e., amplitude, response spectrum, and duration) of an aftershock from statistical data and by selecting ground motions that matched key parameters with the target aftershock. The following conclusions can be drawn based on this work.

(1) Regional seismic damage of buildings under an MS–AS sequence could be predicted reasonably and accurately by city-scale nonlinear THA.

(2) An MS–AS sequence could be generated reasonably by the proposed MS–AS sequence-generation method.

(3) Regional seismic damage of buildings under different MS–AS scenarios could be obtained efficiently by the proposed framework to provide a useful reference for earthquake emergency response and scientific decision making for earthquake disaster relief.

References

Amadio C, Fragiacomo M, Rajgelj S (2003). The effects of repeated earthquake ground motions on the non-linear response of SDOF systems. Earthquake Engineering & Structural Dynamics, 32(2): 291–308

Ancheta T D, Darragh R B, Stewart J P, Seyhan E, Silva W J, Chiou B S J, Wooddell K E, Graves R W, Kottke A R, Boore D M, Kishida T, Donahue J L (2014). NGA-West2 database. Earthquake Spectra, 30 (3): 989–1005

Applied Technology Council (1985). Earthquake damage evaluation data for California. Final Report. Redwood City, CA: Applied Technology Council

Bommer J J, Martínez-Pereira A (1999). The effective duration of earthquake strong motion. Journal of Earthquake Engineering, 3(2): 127–172

Bommer J J, Stafford P J, Alarcón J E (2009). Empirical equations for the prediction of the significant, bracketed, and uniform duration of earthquake ground motion. Bulletin of the Seismological Society of America, 99(6): 3217–3233

CESMD (2019a). Berkeley Earthquake of 20 Oct 2011 (4.0 Mw, 14:41:04 PM PDT, 37.86 N 122.25 W, Depth 8.0 km). CESMD Internet Data Report

CESMD (2019b). Berkeley Earthquake of 20 Oct 2011 (3.8 Mw, 20:16:05 PM PDT, 37.87 N 122.25 W, Depth 9.6 km). CESMD Internet Data Report

Chen H, Xie Q C, Li Z Q, Xue W, Liu K (2017). Seismic damage to structures in the 2015 Nepal earthquake sequences. Journal of Earthquake Engineering, 21(4): 551–578

Chiou B, Darragh R, Gregor N, Silva W (2008). NGA project strong-motion database. Earthquake Spectra, 24(1): 23–44

Du W Q, Wang G (2017). Prediction equations for ground-motion significant durations using the NGA-West2 database. Bulletin of the Seismological Society of America, 107(1): 319–333

Federal Emergency Management Agency (FEMA) (2012). Multi-Hazard Loss Estimation Methodology—Earthquake Model, HAZUS–MH 2.1 Technical Manual. Washington DC: Department of Homeland Security, Federal Emergency Management Agency, Mitigation Division

Fragiacomo M, Amadio C, Macorini L (2004). Seismic response of steel frames under repeated earthquake ground motions. Engineering Structures, 26(13): 2021–2035

Goda K (2012). Nonlinear response potential of mainshock–aftershock sequences from Japanese earthquakes. Bulletin of the Seismological Society of America, 102(5): 2139–2156

Goda K, Salami M R (2014). Inelastic seismic demand estimation of wood-frame houses subjected to mainshock–aftershock sequences. Bulletin of Earthquake Engineering, 12(2): 855–874

Goda K, Taylor C A (2012). Effects of aftershocks on peak ductility demand due to strong ground motion records from shallow crustal earthquakes. Earthquake Engineering & Structural Dynamics, 41 (15): 2311–2330

Haddadi H, Shakal A, Huang M, Parrish J, Stephens C, Savage W U, Leith W S (2012). Report on progress at the Center for Engineering Strong Motion Data (CESMD). In: The 15th World Conference on Earthquake Engineering. Lisbon, Portugal, 24–28

Hatzigeorgiou G D, Beskos D E (2009). Inelastic displacement ratios for SDOF structures subjected to repeated earthquakes. Engineering Structures, 31(11): 2744–2755

Hatzivassiliou M, Hatzigeorgiou G D (2015). Seismic sequence effects

on three-dimensional reinforced concrete buildings. Soil Dynamics and Earthquake Engineering, 72: 77–88

Hori M, Ichimura T, Wijerathne L, Ohtani H, Chen J, Fujita K, Motoyama H (2018). Application of high performance computing to earthquake hazard and disaster estimation in urban area. Frontiers in Built Environment, 4: 1

Hosseinpour F, Abdelnaby A E (2017). Effect of different aspects of multiple earthquakes on the nonlinear behavior of RC structures. Soil Dynamics and Earthquake Engineering, 92: 706–725

Hu S, Gardoni P, Xu L (2018). Stochastic procedure for the simulation of synthetic main shock–aftershock ground motion sequences. Earthquake Engineering & Structural Dynamics, 47(11): 2275–2296

Jalayer F, Asprone D, Prota A, Manfredi G (2011). A decision support system for post-earthquake reliability assessment of structures subjected to aftershocks: An application to L'Aquila earthquake, 2009. Bulletin of Earthquake Engineering, 9(4): 997–1014

Jalayer F, Ebrahimian H (2017). Seismic risk assessment considering cumulative damage due to aftershocks. Earthquake Engineering & Structural Dynamics, 46(3): 369–389

Jamnani H H, Amiri J V, Rajabnejad H (2018). Energy distribution in RC shear wall-frame structures subject to repeated earthquakes. Soil Dynamics and Earthquake Engineering, 107: 116–128

Kim B, Shin M (2017). A model for estimating horizontal aftershock ground motions for active crustal regions. Soil Dynamics and Earthquake Engineering, 92: 165–175

Li Q W, Ellingwood B R (2007). Performance evaluation and damage assessment of steel frame buildings under mainshock–aftershock earthquake sequences. Earthquake Engineering & Structural Dynamics, 36(3): 405–427

Lu X Z, Guan H (2017). Nonlinear MDOF models for earthquake disaster simulation of urban buildings. In: Earthquake Disaster Simulation of Civil Infrastructures: From Tall Buildings to Urban Areas. Singapore: Springer, 257–301

Lu X Z, Han B, Hori M, Xiong C, Xu Z (2014). A coarse-grained parallel approach for seismic damage simulations of urban areas based on refined models and GPU/CPU cooperative computing. Advances in Engineering Software, 70: 90–103

Onur T, Ventura C E, Finn W D L (2006). A comparison of two regional seismic damage estimation methodologies. Canadian Journal of Civil Engineering, 33(11): 1401–1409

Pacific Earthquake Engineering Research Center (PEER) (2019). PEER Ground Motion Database. Pacific Earthquake Engineering Research Center

Polese M, Ludovico M D, Prota A, Manfredi G (2013). Damage-dependent vulnerability curves for existing buildings. Advances in Engineering Software, 42: 853–870

Potter S H, Becker J S, Johnston D M, Rossiter K P (2015). An overview of the impacts of the 2010–2011 Canterbury earthquakes. International Journal of Disaster Risk Reduction, 14: 6–14

Raghunandan M, Liel A, Ryu H, Luco N, Uma S (2012). Aftershock fragility curves and tagging assessments for a mainshock-damaged building. In: Proceedings of the 15th World Conference on Earthquake Engineering. Lisbon, Portugal, 23230–23240

Raghunandan M, Liel A B, Luco N (2015). Aftershock collapse vulnerability assessment of reinforced concrete frame structures. Earthquake Engineering & Structural Dynamics, 44(3): 419–439

Rinaldin G, Amadio C (2018). Effects of seismic sequences on masonry structures. Engineering Structures, 166: 227–239

Ruiz-García J, Negrete-Manriquez J C (2011). Evaluation of drift demands in existing steel frames under as-recorded far-field and near-fault mainshock–aftershock seismic sequences. Engineering Structures, 33(2): 621–634

Ruiz-García J, Yaghmaei-Sabegh S, Bojórquez E (2018). Three-dimensional response of steel moment-resisting buildings under seismic sequences. Engineering Structures, 175: 399–414

Steelman J S, Hajjar J F (2009). Influence of inelastic seismic response modeling on regional loss estimation. Engineering Structures, 31 (12): 2976–2987

Valensise G, Tarabusi G, Guidoboni E, Ferrari G (2017). The forgotten vulnerability: A geology- and history-based approach for ranking the seismic risk of earthquake-prone communities of the Italian Apennines. International Journal of Disaster Risk Reduction, 25: 289–300

Varum H, Furtado A, Rodrigues H, Dias-Oliveira J, Vila-Pouca N, Arêde A (2017). Seismic performance of the infill masonry walls and ambient vibration tests after the Ghorka 2015, Nepal earthquake. Bulletin of Earthquake Engineering, 15(3): 1185–1212

Wan Y G, Wan Y K, Jin Z T, Sheng S Z, Liu Z C, Yang F, Feng T (2017). Rupture distribution of the 1976 Tangshan earthquake sequence inverted from geodetic data. Chinese Journal of Geophysics, 60(6): 583–601

Wooddell K E, Abrahamson N A (2014). Classification of main shocks and aftershocks in the NGA-West2 database. Earthquake Spectra, 30 (3): 1257–1267

Xiong C, Lu X Z, Guan H, Xu Z (2016). A nonlinear computational model for regional seismic simulation of tall buildings. Bulletin of Earthquake Engineering, 14(4): 1047–1069

Xiong C, Lu X Z, Lin X C, Xu Z, Ye L P (2017). Parameter determination and damage assessment for THA-based regional seismic damage prediction of multi-story buildings. Journal of Earthquake Engineering, 21(3): 461–485

Xu Z, Lu X Z, Guan H, Han B, Ren A Z (2014). Seismic damage simulation in urban areas based on a high-fidelity structural model and a physics engine. Natural Hazards, 71(3): 1679–1693

Yepes-Estrada C, Silva V, Rossetto T, D'Ayala D, Ioannou I, Meslem A, Crowley H (2016). The global earthquake model physical vulnerability database. Earthquake Spectra, 32(4): 2567–2585

Zhai C H, Ji D F, Wen W P, Lei W D, Xie L L, Gong M S (2016). The inelastic input energy spectra for main shock–aftershock sequences. Earthquake Spectra, 32(4): 2149–2166

Zhai C H, Wen W P, Li S, Chen Z Q, Chang Z W, Xie L L (2014). The damage investigation of inelastic SDOF structure under the mainshock–aftershock sequence-type ground motions. Soil Dynamics and Earthquake Engineering, 59: 30–41

Zheng Y, Ni S D, Xie Z J, Lv J, Ma H S, Sommerville P (2010). Strong aftershocks in the northern segment of the Wenchuan earthquake rupture zone and their seismotectonic implications. Earth, Planets, and Space, 62(11): 881–886